© 2014. Published by The Company of Biologists Ltd | The Journal of Experimental Biology (2014) 217, 1430-1436 doi:10.1242/jeb.092726

METHODS & TECHNIQUES

Simultaneous high-resolution pH and spectrophotometric recordings of oxygen binding in blood microvolumes

Michael Oellermann, Hans-O. Pörtner and Felix C. Mark*

ABSTRACT

Oxygen equilibrium curves have been widely used to understand oxygen transport in numerous organisms. A major challenge has been to monitor oxygen binding characteristics and concomitant pH changes as they occur *in vivo*, in limited sample volumes. Here we report a technique allowing highly resolved and simultaneous monitoring of pH and blood pigment saturation in minute blood volumes. We equipped a gas diffusion chamber with a broad-range fibre-optic spectrophotometer and a micro-pH optode and recorded changes of pigment oxygenation along oxygen partial pressure (P_{O_2}) and pH gradients to test the setup. Oxygen binding parameters derived from measurements in only 15 µl of haemolymph from the cephalopod *Octopus vulgaris* showed low instrumental error (0.93%) and good agreement with published data. Broad-range spectra, each resolving 2048 data points, provided detailed insight into the complex absorbance characteristics of diverse blood types. After consideration of photobleaching and intrinsic fluorescence, pH optodes yielded accurate recordings and resolved a sigmoidal shift of 0.03 pH units in response to changing P_{O_2} from 0 to 21 kPa. Highly resolved continuous recordings along pH gradients conformed to stepwise measurements at low rates of pH changes. In this study we showed that a diffusion chamber upgraded with a broad-range spectrophotometer and an optical pH sensor accurately characterizes oxygen binding with minimal sample consumption and manipulation. We conclude that the modified diffusion chamber is highly suitable for experimental biologists who demand high flexibility, detailed insight into oxygen binding as well as experimental and biological accuracy combined in a single setup.

KEY WORDS: Diffusion chamber, Oxygen equilibrium curve, Hemocyanin, Haemocyanin, Haemoglobin, pH optode, Octopus, Amphipod, Antarctic fish

INTRODUCTION

Since the first oxygen binding experiments by Paul Bert (Bert, 1878) and Carl Gustav von Hüfner (Hüfner, 1890) and the pioneering work by Bohr, Hasselbalch and Krogh (Bohr et al., 1904) dating back more than a century, oxygen binding experiments have served to understand human blood physiology and diseases (e.g. Chanutin and Curnish, 1967; Festa and Asakura, 1979) or the environmental adaptation of various organisms (e.g. Brix, 1983; Herbert et al., 2006; Meir et al., 2009; Scott, 2011), and have even resolved crime (Olson et al., 2010). Ever since, researchers have developed and refined techniques to comprehend the complex physiology of oxygen transport, leading to a variety of currently employed methods (supplementary material Table S1).

Alfred Wegener Institute for Polar and Marine Research, 27570 Bremerhaven, Germany.

*Author for correspondence (FMark@awi.de)

Received 18 June 2013; Accepted 9 January 2014

Such analysis commonly involves the determination of oxygen affinity (P_{50}). Accurate determination of P_{50} requires the control or monitoring of extrinsic factors such as temperature, carbon dioxide and particularly pH. Assessing the effects of pH and the variation of pH during transition from the oxygenated to the deoxygenated state, due to the oxygenation-dependent release or uptake of protons by the pigment (Haldane effect), requires knowledge of pH at different levels of saturation for the analysis of oxygen equilibrium curves (OECs). Conventionally, experimenters control pH by added buffers [e.g. Tris, HEPES (Brix et al., 1994)] or determine pH from sub-samples or separately conditioned samples (e.g. Seibel et al., 1999; Weber et al., 2008) and rarely directly in the original sample (Pörtner, 1990; Zielinski et al., 2001). While added buffers prevent pH changes and may help to address specific functional characteristics of the pigment [e.g. effects of inorganic ions (Mangum and Lykkeboe, 1979)], they disturb the fine tuning of oxygen binding (Brix et al., 1994) and block pH changes relevant as part of the oxygen transport process, which need to be included for a comprehensive picture of oxygen transport *in vivo*. A major challenge in monitoring pH has been the relatively large sample volume required to immerse a pH electrode and its reference electrode. Particularly, analysis in highly limited sample volumes or devices that employ thin blood films (e.g. diffusion chamber, HemOscan, Pwee 50; supplementary material Table S1) suffer from this constraint.

Further, while many commercially available devices have been designed for mammalian (including human) blood analysis (e.g. CO-Oximeter, HEMOX-Analyser), only few provide the flexibility needed for the analysis of non-model organism blood, characterized by small sample volumes, unusual spectra, extreme *in vitro* temperatures or high pH sensitivity.

Here we report a major step forward in the respective methodology, allowing the simultaneous analyses of pH and pigment absorbance in microvolumes of blood. The challenges successfully met by our technique comprise: (1) the parallel measurement of oxygenation, paired with the simultaneous monitoring of pH depending on oxygenation level; (2) the use of minimal sample volumes of 15 µl; and (3) high-resolution recordings, facilitated by continuous recordings of broad-range spectra and pH.

We upgraded a gas diffusion chamber (Niesel and Thews, 1961; Sick and Gersonde, 1969; Sick and Gersonde, 1972; Bridges et al., 1984; Morris and Oliver, 1999; Weber et al., 2010) with an integrated fibre-optic micro-pH optode and a miniature broad-range fibre-optic spectrophotometer. The experimental setup offers high flexibility to produce accurate OECs and pH recordings from only minute volumes of sample.

RESULTS AND DISCUSSION

Spectrophotometric measurements

Using the modified diffusion chamber, we successfully performed measurements on haemolymph from *Octopus vulgaris* and

The Journal of Experimental Biology

The Journal of Experimental Biology (2014) doi:10.1242/jeb.092726

List of symbols and abbreviations

n_{50}	Hill coefficient
OEC	oxygen equilibrium curve
P_{50}	oxygen affinity
P_{CO_2}	carbon dioxide partial pressure
P_{O_2}	oxygen partial pressure

Eulimnogammarus verrucosus and whole blood of *Pachycara brachycephalum* at various oxygen and carbon dioxide partial pressures (P_{O_2} and P_{CO_2}, respectively) and temperatures. The integrated broad-range spectrophotometer resolved 2048 data points per spectrum from 200 to 1100 nm and yielded characteristic absorbance spectra for haemolymph containing haemocyanin with an oxygenation-dependent peak at 347 nm (*O. vulgaris*; Fig. 1A), and multiple responsive peaks at 540, 575, 412 and 335 nm for oxygenated haemoglobin-bearing blood and at 553, 427 and 366 nm for deoxygenated haemoglobin-bearing blood (*P. brachycephalum*; Fig. 1B). In addition, to the haemocyanin peak at 336 nm, haemolymph from *E. verrucosus* showed absorbance features above 400 nm that explain its green coloration (Fig. 1C). The detailed broad-range spectra strongly facilitate and enhance the analysis of solutions with complex absorbance spectra. Studies that gather only snapshots of the spectrum by means of single wavelength filters (e.g. Morris et al., 1985; Rasmussen et al., 2009) limit their experimental setup to a particular pigment type and may miss further relevant features.

The modified diffusion chamber yielded reproducible and accurate results employing both conventional stepwise measurements along an oxygen partial pressure (P_{O_2}) gradient (Fig. 2) as well as measurements along a pH gradient (Fig. 3), designed for pH-sensitive pigments such as cephalopod haemocyanins (Pörtner, 1990). OECs of *O. vulgaris* haemolymph constructed from five replicated experiments with discrete oxygenation steps at constant P_{CO_2} (1 kPa) showed low variability among OECs and the derived parameters (Fig. 2, Table 1; supplementary material Fig. S1), with a relative error of 0.93% for P_{50} and 2.74% for the Hill coefficient, n_{50}. This low instrumental error and the good agreement of P_{50} and n_{50} with published data on *O. vulgaris* haemolymph recorded at the same temperature and pH (Table 1, Fig. 4) underline the accuracy of the setup. The Bohr coefficient recorded at 15°C was higher than that reported in Brix et al. (Brix et al., 1989), but closely matched values reported for *O. vulgaris* by Houlihan et al. (Houlihan et al., 1982) and Bridges (Bridges, 1995) *Octopus dofleini* [−1.7; pH 7.0–8.3 (Miller, 1985)] or *Octopus macropus* [−1.99; pH 7.3–7.5 (Lykkeboe and Johansen, 1982)] (Fig. 4, Table 1). The difference in Bohr coefficients with those in the study by Brix et al. (Brix et al., 1989) relates to the pH ranges used to determine the Bohr coefficient. In octopods, P_{50} increases linearly with pH and levels off at lower pH (~7.0; Fig. 4) (Miller, 1985) as oxygen binding becomes pH insensitive (see 13 kPa OEC, Fig. 3). Brix et al. (Brix et al., 1989) included pH values below 7.0 (6.85–7.40), which consequently led to reduced regression slopes and underestimated Bohr coefficients. Thus, agreement with studies using pH ranges above 7.0 confirms the accuracy of Bohr coefficients determined with the modified diffusion chamber.

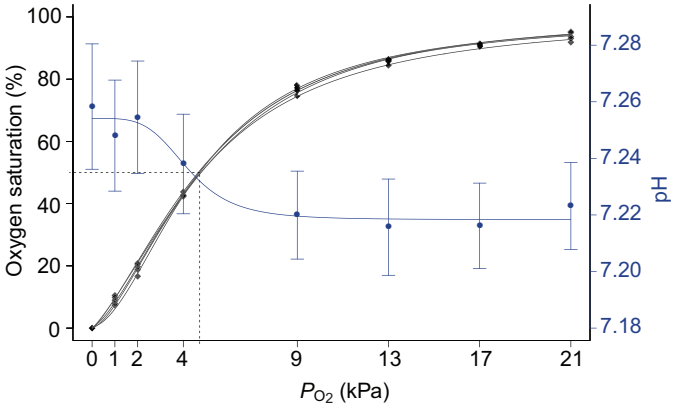

Fig. 2. Replicated (*n*=5) oxygen equilibrium curves of haemolymph from one *Octopus vulgaris* specimen obtained by stepwise changes to discrete P_{O_2} at constant P_{CO_2} (1 kPa). Five parameter logistic curves were fitted and individually plotted for each measurement to illustrate instrumental variability. Haemolymph pH (means ± s.e.m., blue), recorded by an optical pH microsensor immersed in the same sample droplet, changed sigmoidal and reverse directional to pigment saturation (black). The pH at half saturation (mean ± s.e.m.=7.23±0.018) can be derived from the intersection between P_{50} (dashed line) and the fitted pH line.

Both pigment absorbance and haemolymph pH responded to changes in gas composition within 30 s (Fig. 5). The recording of one OEC, including calibration at 100% and 0% oxygen saturation, lasted on average 3.5±0.23 h for measurements (*n*=5) with eight discrete oxygenation steps and 5.2±0.21 h for measurements (*n*=4) with eight discrete pH steps. While the maximum absorbance signal at 347 nm (haemocyanin oxygenation peak) drifted by −3.5±0.6% per hour (*n*=5), minimal absorbance remained nearly constant (0.27±0.21%, *n*=5). The protein peak drifted less and varied more

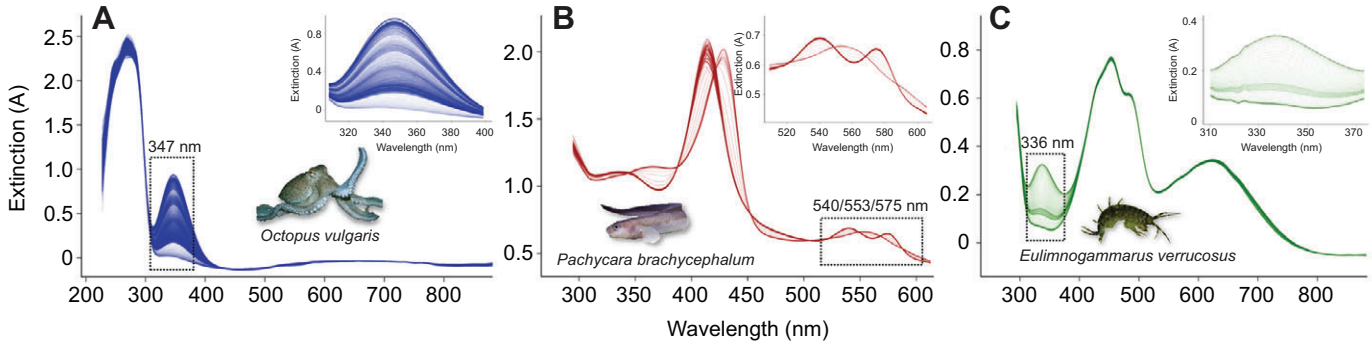

Fig. 1. Highly resolved spectral changes of several non-model organisms. (A) Broad-range spectra of haemolymph from *Octopus vulgaris* (15°C), measured at 4 kPa P_{O_2} from high to low pH (ca. 8.2–6.8). Exemplary, broad-range spectral recordings of whole blood from (B) the Antarctic eelpout *Pachycara brachycephalum* (0°C) and (C) of haemolymph from the Lake Baikal amphipod *Eulimnogammarus verrucosus* (6°C) reveal complex absorbance features. Spectral zones responding to oxygenation are marked by boxes and magnifications are shown in the insets. Spectra were coloured according to the visual appearance of the respective haemolymph/blood type. (Animal photos reprinted with permission by: Vladimír Motyčka, Christoph Held and Lena Jakob.)

The Journal of Experimental Biology (2014) doi:10.1242/jeb.092726

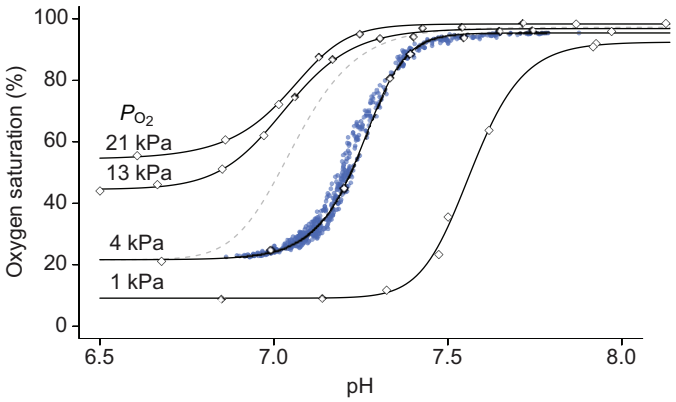

Fig. 3. Stepwise oxygen equilibrium curves (OECs) along a pH gradient (Pörtner, 1990), each derived from 15 µl *Octopus vulgaris* haemolymph and measured by means of the modified diffusion chamber at 15°C and decreasing pH and various constant P_{O_2} (1, 4, 13 and 21 kPa). The continuous OEC recorded at slow rates of P_{CO_2} changes (0.015 kPa min^{-1}, blue points) was highly resolved and closely matched the stepwise curves, while at faster rates the OEC shifted left (dashed grey curve).

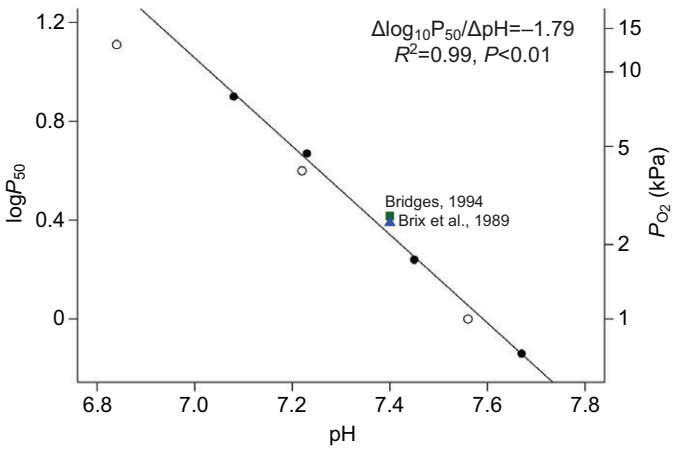

Fig. 4. Bohr plot illustrating the pH dependence of oxygen affinity (P_{50}) of *Octopus vulgaris* haemolymph measured at 15°C. P_{50} from experiments with stepwise changes of P_{O_2} (filled circles) and pH (open circles) agreed with literature data [blue triangle (Brix et al. 1989); green square (Bridges, 1995)]. The data point at 13 kPa was excluded from the linear regression fit as P_{50} leveled off at low pH (~7.0).

among experiments (2.3±2.7%, n=5; Fig. 5B). Negative drift observed for the maximum oxygenation signal was reported previously and explained by autoxidation of the blood pigment (Wells and Weber, 1989). Consequently, each measurement needs to comprise calibration steps with pure oxygen at the beginning and end to determine and include the apparent and constant drift in the calculation of pigment oxygenation by readjusting maximum absorbance at each consecutive oxygenation step (Wells and Weber, 1989). The less pronounced positive drift of the protein peak (Fig. 5B) indicates a low degree of sample drying and no apparent dilution by condensation or denaturation of the haemolymph sample.

Interestingly, the height of the protein peak did not remain stable, but increased/decreased upon oxygenation/deoxygenation (Fig. 5; supplementary material Fig. S2). This unexpected response of the protein peak to oxygenation/deoxygenation of the pigment (Fig. 5; supplementary material Fig. S2) cannot be ascribed to irreversible protein denaturation as the protein absorbance increased again upon re-oxygenation. Consequently, oxygenation status may affect protein absorbance spectra and thus measurements of protein concentration in haemolymph or blood. Conformational changes depending on the degree of oxygenation may affect the absorbance features of the aromatic tryptophan, tyrosine and phenylalanine residues that account for the absorbance at 270–295 nm (Alexander and Ingram, 1980). Although the protein peak may not always vary with oxygen content (Bolton et al., 2009), it would be advisable to test a given blood type for such oxygenation dependency.

pH recordings in blood microvolumes

Simultaneous monitoring of pH, using a pH micro-optode in the same 15 µl sample, yielded stable recordings within the calibrated range between pH 6.5 and 8.2. In response to changing P_{O_2} (0–21 kPa), these recordings were sufficiently precise to resolve a sigmoidal shift by 0.03 pH units, running in reverse to the OEC (Fig. 2). This shift denotes the oxygenation-dependent, lowered affinity of the pigment for protons (Haldane effect) and agrees well with other studies [e.g. *Carcinus maenas* ΔpH=0.02 (Truchot, 1976)]. A sigmoidal rather than linear change of pH (Lapennas et al., 1981) may correspond to the linked sigmoidal trajectory of

Table 1. Comparison of blood physiological parameters of *Octopus vulgaris* haemolymph with literature data

Source	P_{50} (kPa)	n_{50}	Bohr coefficient	pH	Temperature (°C)
Present study	0.72	1.56	**–1.79** (pH 7.1–7.7)	7.68	15
	1.72	1.59		7.45	
	4.72 (0.07)	1.75 (0.07)		7.23 (0.046)	
	7.94	1.61		7.08	
	2.20[a]	–		7.4	
Brix et al., 1989	**2.45**	1.5	**–1.34** (pH 6.85–7.4)	7.4	15
	4.41	1.6	−1.10 (pH 6.85–7.4)	7.4	25
Houlihan et al., 1982	3.20	2.6[b]	−1.58/−1.73 (pH 7.2–7.6/7.3–7.7)	7.588	22
	4.09	2.9[b]		7.520	
	4.80	3.5[b]		7.415	
	6.76	2.9[b]		7.327	
Bridges, 1995	1.91	–	−1.86	7.4	10
	2.61	–	**–1.83**	7.4	15

P_{50}, oxygen affinity; n_{50} Hill coefficient. Bold values denote parameters recorded under the same conditions. Values in parentheses for P_{50}, n_{50} and pH represent ±95% confidence intervals.

[a]P_{50} extrapolated from linear regression line of Bohr plot at pH 7.4 (Fig. 4).

[b]Hill coefficients were recalculated from Houlihan et al. (Houlihan et al., 1982).

The Journal of Experimental Biology (2014) doi:10.1242/jeb.092726

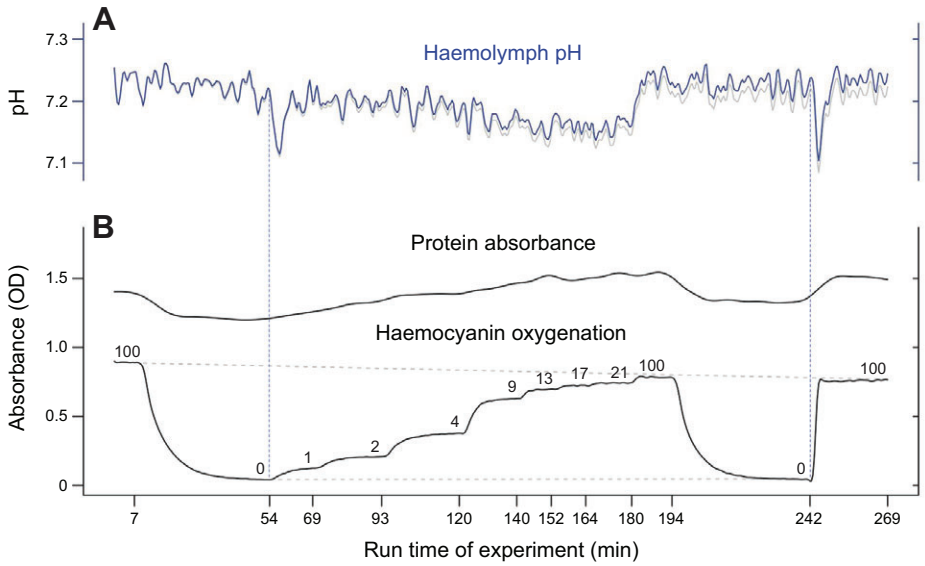

Fig. 5. Change of haemolymph pH and wavelength-specific absorbance during an oxygen equilibrium measurement. Response of (A) pH (uncorrected, grey trace; corrected by instrumental pH drift, blue trace) and (B) absorbance of the oxygenation-dependent peak (347 nm) and the protein peak of *Octopus vulgaris* haemolymph to stepwise changes of P_{O_2} recorded at 15°C. Numbers above the absorbance trace indicate P_{O_2} (kPa) of each oxygenation step. Horizontal dashed lines indicate the change of maximal and minimum absorbance (at 347 nm) over time, and vertical dashed lines the sudden but reversible pH changes upon initial oxygenation.

oxygen binding. The continuous recording of pH further revealed pronounced but reversible decreases of ~0.1 pH units upon initial oxygenation, which indicates a high affinity state for protons in fully deoxygenated haemocyanins (Fig. 5).

P_{50} derived from OECs recorded along pH gradients matched those recorded along P_{O_2} gradients and together showed a linear interdependence of pH and P_{50} in the pH range between 7.1 and 7.7 (Fig. 4). The OEC recorded by a continuous decrease of pH was highly resolved (~500 data points; Fig. 6) and fully equilibrated at slow P_{CO_2} changes of 0.015 kPa min^{-1}, as confirmed by the close match with the stepwise OEC (Fig. 3). This further underlines the validity of this alternative methodology, designed for pH-sensitive pigments. Simultaneous pH recordings, as in the present study, allow construction of highly resolved, continuous OECs from which blood parameters may be directly derived without curve modelling (Fig. 3). At faster rates (0.045 kPa min^{-1}), the OEC shifted left as saturation required longer to stabilize than pH (Fig. 3). A shift of continuous OEC at higher rates of change of P_{CO_2} or P_{O_2} has been explained by dislike equilibration rates with the surrounding gas between the sensor and the sample, due to differences in their physical properties or their relative position [‘dynamic error’ (Lapennas et al., 1981)]. However, as the pH optode was immersed in the sample, gas diffusion rates between the sample and the sensor were likely similar, suggesting some delay in oxygenation of octopus haemocyanin in response to pH changes.

The signal of the pH optode drifted by −0.016 pH units per 100 recordings (±0.004) and was corrected accordingly (Fig. 5A). This drift was higher than stated by the manufacturer (−0.0035 pH units per 100 recordings) (PreSens, 2004; PreSens, 2012), probably because of incomplete protection from the light beam of the UV-VIS light source and resulting photobleaching of the optode’s fluorescent dyes. Thus, pH optodes may be re-calibrated prior to each measurement and the pH signal corrected for instrumental signal drift. Light exposure and therefore pH signal drift can be reduced by a software-controlled shutter in the light path that opens only during measurements or by using optically isolated sensor tips. The pH signal was also corrected for autofluorescence emitted by the sample, which decreased the pH signal in haemolymph by 0.06 units. Optical isolation but also calibration in the analysed medium can reduce or prevent the effects by intrinsic fluorescence between 530 and 660 nm, caused by, for example, porphyrine structures, which affect phase and amplitude of the pH raw signal (PreSens, C. Krause, personal communication).

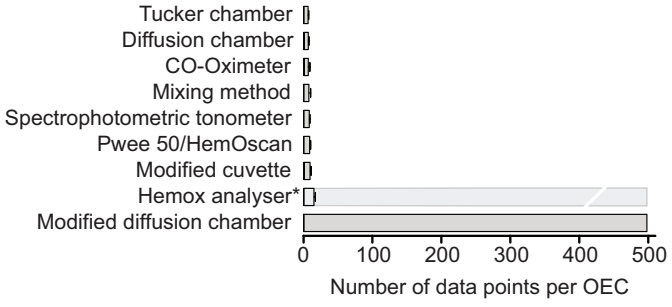

Fig. 6. Number of data points (means ± 95% CI) for single oxygen equilibrium curves (OECs) compared between different methods (for references, see supplementary material Table S2). The modified diffusion chamber method refers to continuous OEC measurements along a pH gradient. *While some studies record fewer data points, recording intervals may be maximized to 1 s^{-1}.

Advantages and disadvantages

The modified diffusion chamber benefits the analysis of oxygen binding in several ways. Simultaneous recording of pigment oxygenation and pH allows characterization of oxygen binding and intrinsic pH responses under conditions mimicking *in vivo* conditions. Minute sample volumes facilitate the analysis of blood from small organisms or less invasive and repeated sampling from the same individual. Small sample volumes reduce the need to pool blood, facilitate replicate measurements and shorten measurement time because of accelerated gas equilibration. Highly resolved broad-range spectra capture detailed spectral properties of the pigment and promote the analysis of diverse blood types. Thin optical microsensors (for pH or P_{O_2}) deliver stable and rapid recordings down to 0°C (M.O., unpublished observation) and allow recording of continuous and highly resolved OECs (Fig. 3). The gain of detail improves the accuracy of biophysical oxygen binding models, particularly if OECs do not follow a simple sigmoidal shape (Wells and Weber, 1989). The additional flexibility to operate at a large range of experimental temperatures and gas compositions makes this device not only highly suitable for standard applications

The Journal of Experimental Biology (2014) doi:10.1242/jeb.092726

but particularly for the functional analysis of blood from non-model organisms.

The use of optical microsensors and thin layers of blood also require specific care. The fluorescent dyes of the pH optodes are prone to photobleaching, which can be overcome by optical isolation or determination and correction for signal drift. Effects of intrinsic fluorescence of the sample are resolved by optical isolation, calibration in the same type of sample or by an initial cross-validation of pH with a pH electrode. The non-linear dynamic range of pH optodes restricts accurate recordings to pH values between 5.5 and 8.5, which, however, suffices in most of the blood-physiological experiments. Optical pH sensors that cover the extreme and even the full pH range may soon remove this limitation (Safavi and Bagheri, 2003). Further, the 150 µm sensor tip breaks easily and requires careful handling. Like pH electrodes, pH optodes require calibration with buffers of similar ionic strength as the sample analysed and at the same experimental temperature (PreSens, 2004). Some blood types may clog on the sensor tip, which can be avoided by bathing the pH optode in a heparin solution (1000 units ml^{-1}). Lastly, thin layers of blood are at higher risk of dessication (Reeves, 1980), particularly at higher temperatures. Measures to avoid dessication include decreased gas flow or covering of the blood sample with a gas permeable Teflon membrane (Reeves, 1980; Lapennas and Lutz, 1982; Clark et al., 2008).

Conclusions

In this study we showed that a diffusion chamber upgraded with a broad-range spectrophotometer and a fibre-optical pH sensor allows for parallel measurement of pH and pigment saturation in microvolumes of blood samples. The setup yields reproducible and accurate results and offers high flexibility regarding the type of samples and experimental setting. The availability of optical P_{O_2} or P_{CO_2} probes and the rapid development of other optical sensor types (e.g. nitrogen oxide) suggest a broad array of future implementations that will help to address novel biological questions.

MATERIALS AND METHODS

Experimental setup and modifications

A gas diffusion chamber (Eschweiler Co., Kiel, Germany) designed and described in detail previously (Niesel and Thews, 1961; Sick and Gersonde, 1969; Sick and Gersonde, 1972) has been used to determine OECs by recording absorbance of a thin layer of a haemoglobin- or haemocyanin-bearing solution during continuous or stepwise changes of P_{O_2} (Wells and Weber, 1989). The original principle, characterized by full pigment deoxygenation with nitrogen gas followed by the time-dependent diffusion of oxygenated gas into the chamber (Niesel and Thews, 1961; Sick and Gersonde, 1969), was essentially abolished in subsequent studies that continuously perfused the chamber with defined gas mixtures (e.g. Bridges et al., 1984; Morris and Oliver, 1999; Weber et al., 2010). We adopted this amendment and further modified the diffusion chamber as follows. (1) A broad-range (200 to 1100 nm) fibre-optic spectrophotometer (USB2000+, Ocean Optics, USA) was connected via two fibre-optic cables fitted to the central cylinder of the diffusion chamber to direct the light beam via collimating lenses from the deuterium halogen light source (DT-Mini-2-GS, Ocean Optics) through the sample glass plate back to the 2048-element CCD-array detector of the spectrophotometer (Fig. 7; supplementary material Table S3). (2) The plastic slide that holds the sample glass plate in the light tunnel was modified to fit a fibre-optic micro-pH optode (NTH-HP5-L5-NS*25/0.8-OIW, PreSens, Germany), housed in a syringe and connected to a phase detection device (µPDD 3470, PreSens; Figs 7, 8). The needle of the syringe was then inserted through a silicone ring to prevent the leakage of gas (Fig. 8). In contrast to pH electrodes, pH optodes exhibit very small sensor tips (<150 µm) and determine pH from the intensity ratio between two pH-sensitive fluorescent dyes (PreSens, 2004). The modified diffusion chamber has been registered under patent number 10 2013 011 343 at the Deutsches Patent- und Markenamt, Germany.

The water reservoir of the diffusion chamber was filled with a 20% ethylene glycol solution (anti-freeze agent, AppliChem, Germany) and the temperature was monitored and controlled by means of a supplied temperature sensor (PreSens, Germany) and a connected circulating thermostatted water bath (LAUDA Ecoline Staredition RE 104, Germany). A gas mixing pump (Wösthoff, Germany) supplied an adjustable mixture of nitrogen, oxygen and carbon dioxide gas, humidified by an integrated scrubber to prevent desiccation of the sample (Fig. 8).

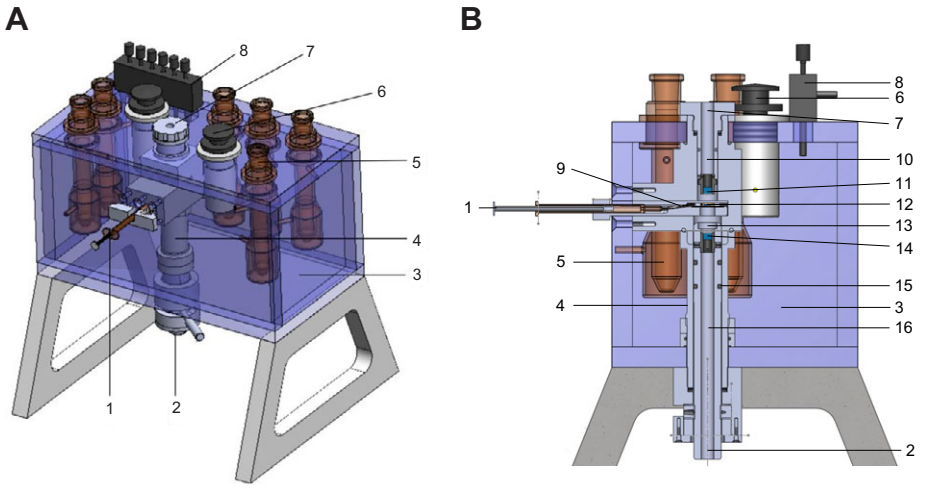

Fig. 7. Illustration of the modified diffusion chamber. (A) 3D model of the modified diffusion chamber and (B) a detailed cross-section through the central cylinder of the gas diffusion chamber illustrating the embedded fibre-optic micro-pH optode and an upper and lower custom-made tube containing collimating lenses and fittings for incoming and outgoing fibre-optic cables of the light source and the broad-range spectrophotometer. 1, Syringe housing for the pH micro optode; 2, fibre-optic cable exit to the spectrophotometer; 3, temperature-controlled water reservoir; 4, central cylinder containing optical devices; 5, gas-washing flask; 6, control wheel for gas distribution; 7, fibre-optic cable inlet from the light source; 8, control panel for gas inflow; 9, needle housing for the fibre-optic sensor tip; 10, upper custom-made tube, housing a collimating lens and the fibre-optic cable from the light source; 11, upper collimating lens; 12, blood sample spread on a glass plate; 13, spacer to keep 10 mm minimal distance between collimating lens and sample; 14, lower collimating lens; 15, rubber to seal lower tubing; 16, lower custom-made tube, housing a collimating lens and the fibre-optic cable leading to the spectrophotometer. Illustrations were drawn with 3D CAD software (SolidWorks, version 12.0; files available at http://doi.pangaea.de/10.1594/PANGAEA.831205).

The Journal of Experimental Biology (2014) doi:10.1242/jeb.092726

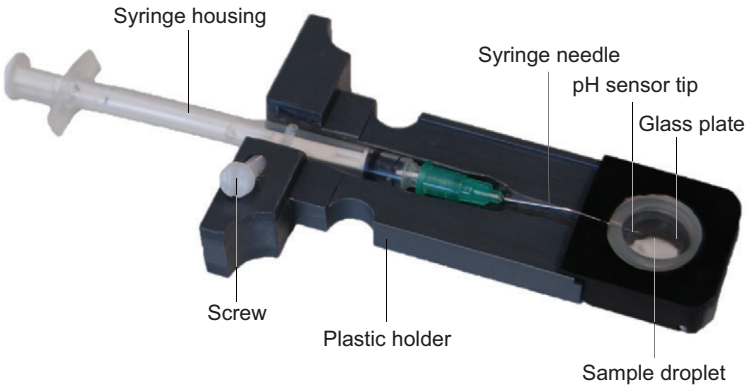

Fig. 8. Detailed illustration of the pH optode housed in a syringe, mounted with a screw and fitted to a plastic holder, which is moved into the gas-tight compartment centred in the diffusion chamber. The bended syringe needle is inserted through a silicon ring, which prevents gas leakage, and the sensor tip moved into the edge of the sample droplet located on a silica glass plate.

Prior to each experiment, we performed a six-point calibration (pH 6.7, 7.0, 7.2, 7.4, 7.7 and 8.1) of the pH optode, in MOPS-buffered [40 mmol l^{-1}, 3-(*N*-morpholino)-propanesulfonic acid], filtered artificial seawater (35 PSU) at the corresponding experimental temperature. pH of buffers was checked with a pH glass electrode (InLab Routine Pt1100, Mettler Toledo, Germany) and a pH meter (pH 330i, WTW, Germany), calibrated with low ionic strength pH standards (AppliChem, Germany, DIN19266) and corrected to the free scale pH with Tris-buffered seawater standard (CO_2 QCLab, batch 4 2010, Dickson, USA) (Dickson, 2010) equilibrated at the same temperature. Aliquots of 18 µl of haemolymph (octopus or amphipod) were thawed on ice, shortly spun down to collect content (5 s at 1000 ***g***), and 0.35 µl of 0.2 mmol l^{-1} NaOH (4.6 µmol l^{-1} final concentration) was added to raise haemolymph pH above 8.0 to ensure full pigment oxygenation. To avoid haemolysis and the formation of methaemoglobin by freezing, we used freshly sampled whole blood from *P. brachycephalum* and diluted the sample with one volume of blood plasma to improve light transmission during the measurement. The pH of haemolymph or whole blood was not stabilized with extrinsic buffers such as Tris or HEPES as they disturb the effects by ligands and temperature on pigment oxygenation (Brix et al., 1995). We then spread out 15 µl of haemolymph or whole blood on the glass plate without contacting the sealing ring. The pH optode needle was inserted through the sealing ring and the sensor tip moved into the edge of the droplet to reduce bleaching of the dye by the light beam passing through the centre of the glass plate (Fig. 8). Both the glass plate holder and the fitted pH optode were then inserted and fixed in the diffusion chamber (Fig. 7). The spectrophotometer required the recording of light and dark spectra without blood sample before each measurement and was set to 15 ms integration time, averaging 100 scans per recording and 30 s measurement intervals. pH drift of the pH optode was evaluated by measuring the pH difference of a MOPS-buffered seawater pH standard (pH 7.2) at 15°C before and after each experiment. Effects of intrinsic fluorescence were assessed by comparing pH recordings of the pH optode and the pH electrode in octopus haemolymph at 15°C.

Using *O. vulgaris* haemolymph, we tested the setup via two previously employed methodologies. OECs were obtained (1) by stepwise changes of discrete P_{O_2} (1, 2, 4, 9, 13, 17 and 21 kPa) at constant P_{CO_2} (e.g. Wells and Weber, 1989) or (2) by stepwise as well as continuous decreases of pH by means of increasing CO_2 concentrations (0–20 kPa) and constant P_{O_2} (e.g. Pörtner, 1990). While stepwise measurements allow the sample to fully equilibrate at several successive but discrete P_{O_2} or pH steps (Lapennas et al., 1981; Pörtner, 1990), continuous measurements characterize a constant change and monitoring of P_{O_2} or pH (Wells and Weber, 1989). Each experiment involved calibration with pure nitrogen as well as pure oxygen at the beginning and at the end to determine the drift of the maximum absorbance signal. The exemplary analysis of whole blood of *P. brachycephalum* was performed from 21 to 0 kPa P_{O_2} and pH 8.2–7.1 at 0°C and of thawed haemolymph of *E. verrucosus* at a constant P_{O_2} of 21 kPa and pH 7.7–6.9 at 6°C.

Animals

One major incentive to advance this method was to enhance the investigation of non-model organisms, which often suffer from instrumental restrictions (e.g. sample volume, wavelength filters, temperature setting) by devices optimised for human or rodent blood. We thus chose three non-model organisms with diverse experimental demands to test the flexibility and accuracy of the modified diffusion chamber. The cephalopod *Octopus vulgaris* Cuvier 1797 lives between 11 and 18°C and has evolved a closed circulatory system containing blue haemolymph with high concentrations [54.3±6.9 g l^{-1} (Wells and Smith, 1987; Brix et al., 1989)] of the extracellular, pH-sensitive respiratory pigment haemocyanin, which evolved independently from arthropod haemocyanin (van Holde et al., 2001). Published data on *O. vulgaris* blood physiology allowed us to test the accuracy of the modified diffusion chamber. The Antarctic eelpout *Pachycara brachycephalum* (Pappenheim 1912) lives at freezing temperatures, yields only little blood and circulates intracellular haemoglobin at – for teleosts – low concentrations (37.4 g l^{-1}) in a closed system. The Baikal amphipod *Eulimnogammarus verrucosus* (Gerstfeldt 1858) lives at 5–6°C and yields small amounts of green haemolymph that transports oxygen via extracellular haemocyanin (45.3±7.9 g l^{-1}) in an open vascular system (Wirkner and Richter, 2013).

Octopus vulgaris specimens were hand-caught by snorkelling at Banuyls sur Mer, France, at 16°C. Animals were anaesthetized in 3% EtOH (Ikeda et al., 2009), and after withdrawing haemolymph from the cephalic vein, were finally killed by a cut through the brain following sampling. *Pachycara brachycephalum* was caught on the Polarstern cruise ANTXXV/4 near Maxwell Bay at King George Island, Antarctica, in May 2009 using fish traps, transported to the Alfred Wegener Institute, Bremerhaven, Germany, and kept in aerated tanks connected to a re-circulating aquaculture system at 0°C. The animal was anaesthetised with 0.3 g l^{-1} tricaine methanosulphonate, blood was withdrawn using a heparinized syringe and the animal was finally killed by a spinal cut [animal research permit no. 522-27-11/02-00(93), Freie Hansestadt Bremen, Germany]. *Eulimnogammarus verrucosus* was collected in Bolshie Koty, Lake Baikal, Russia, during summer 2012, transported to Irkutsk, Russia, and kept in aerated 2.5 l tanks at 6°C. Haemolymph was withdrawn using a dorsally inserted capillary. All haemolymph samples were centrifuged at 15,000 ***g*** for 15 min at 0°C to remove cell debris and stored at −20°C.

Data analysis

The processing, time-matching and analysis of data from both the spectrophotometer and the pH meter were performed using the R statistical language (R Development Core Team, 2013) (for R scripts, see http://doi.pangaea.de/10.1594/PANGAEA.831205).

An integrated five-parameter logistic model [Eqn 1; R 'drc' add-on package (Ritz and Streibig, 2005)] was applied to fit sigmoidal curves to stepwise OECs:

$$f[x,(b,c,d,e,f)] = c + \frac{(d-c)}{\left(1+\exp\left\{b\left[\log\left(\frac{x}{e}\right)\right]\right\}\right)^{f}}. \quad (1)$$

The parameters *c* and *d* denote the upper and lower asymptotes, respectively, and *f* the asymmetry of the curve. The parameters *b* and *e* correspond to the slope and inflection point, respectively, of a four-parameter logistic model if the parameter *f* equals 1. Note that this equation represents an empirical curve fit that does not describe the functional properties of the haemocyanin sub-units according to mechanistic insight.

Oxygen affinity (P_{50}) was interpolated from fitted OECs at half saturation and cooperativity (Hill's coefficient, n_{50}) was determined via Hill plots by regressing $\log_{10}[Y/(1–Y)]$ versus $\log_{10}P_{O_2}$ in the linear mid-range (~20–80%

saturation), with Y denoting the fractional saturation. The Bohr coefficient was calculated from the regression slope ($\Delta\log_{10}P_{50}$ versus ΔpH) between pH 7.1 and 7.7. In pH/saturation diagrams, P_{50} denotes the $\log_{10}$ of the oxygen isobar and the pH of the isobar at half saturation [pH_{50} (Pörtner, 1990)]. Data were expressed as means ± 95% confidence intervals if not stated otherwise.

Acknowledgements
We thank Dr Jan Strugnell (La Trobe University, Bundoora) for providing lab space and her extensive support; Michael Imsic and all other staff and technicians of the La Trobe University for their kind support during the initial tests of the modified diffusion chamber; Erich Dunker, Matthias Littmann and Dirk Wethje (scientific workshop, Alfred Wegener Institute, Bremerhaven) for the technical modifications and drawings of the diffusion chamber; Lena Jakob for providing haemolymph samples from *Eulimnogammarus verrucosus*; Marian Y Hu for his help catching *Octopus vulgaris*; the logistics department of the Alfred Wegener Institute; and last of all Saumya Pant and little Yuva Lalit Pant for their enriching company. We further thank Roy Weber for his kind advice and the two anonymous reviewers for their many helpful remarks and suggestions on an earlier version of this manuscript. We dedicate this article to the memory of Steve Morris and express our special thanks to Maria Morris and Elizabeth Morgan (University of Bristol), who saved and donated the diffusion chamber to our department.

Competing interests
The authors declare no competing financial interests.

Author contributions
M.O. and F.C.M. conceived and developed the technical modifications, compiled the manuscript and interpreted results. M.O. performed the experiments and analysis. H.-O.P. initiated the discussion and contributed to data interpretation and manuscript editing.

Funding
This study was supported by a *Journal of Experimental Biology* travelling fellowship, a PhD scholarship by the German Academic Exchange Service (DAAD, D/11/43882) to M.O., the Deutsche Forschungsgemeinschaft (MA4271/1-2 to F.C.M.) and the Alfred Wegener Institute for Polar and Marine Research.

Supplementary material
Supplementary material available online at
http://jeb.biologists.org/lookup/suppl/doi:10.1242/jeb.092726/-/DC1

References

Alexander, J. B. and Ingram, G. A. (1980). A comparison of five of the methods commonly used to measure protein concentrations in fish sera. *J. Fish Biol.* **16**, 115-122.
Bert, P. (1878). *La Pression Barométrique: Recherches de Physiologie Expérimentale*. Paris: G. Masson.
Bohr, C., Hasselbalch, K. and Krogh, A. (1904). Über einen in biologischer Beziehung wichtigen Einfluss, den die Kohlensäurespannung des Blutes auf dessen Sauerstoffbindung übt. *Skand. Arch. Physiol.* **16**, 402-412.
Bolton, J. C., Collins, S., Smith, R., Perkins, B., Bushway, R., Bayer, R. and Vetelino, J. (2009). Spectroscopic analysis of hemolymph from the American lobster (*Homarus americanus*). *J. Shellfish Res.* **28**, 905-912.
Bridges, C. R. (1995). Bohr and root effects in cephalopod haemocyanins – paradox or pressure in *Sepia officinalis*? *Mar. Freshw. Behav. Physiol.* **25**, 121-130.
Bridges, C. R., Morris, S. and Grieshaber, M. K. (1984). Modulation of haemocyanin oxygen affinity in the intertidal prawn *Palaemon elegans* (Rathke). *Respir. Physiol.* **57**, 189-200.
Brix, O. (1983). Giant squids may die when exposed to warm water currents. *Nature* **303**, 422-423.
Brix, O., Bårdgard, A., Cau, A., Colosimo, A., Condo, S. and Giardina, B. (1989). Oxygen-binding properties of cephalopod blood with special reference to environmental temperatures and ecological distribution. *J. Exp. Zool.* **252**, 34-42.
Brix, O., Colosimo, A. and Giardina, B. (1995). Temperature dependence of oxygen binding to cephalopod haemocyanins: ecological implications. *Mar. Freshw. Behav. Physiol.* **25**, 149-162.
Chanutin, A. and Curnish, R. R. (1967). Effect of organic and inorganic phosphates on the oxygen equilibrium of human erythrocytes. *Arch. Biochem. Biophys.* **121**, 96-102.
Clark, T. D., Seymour, R. S., Wells, R. M. G. and Frappell, P. B. (2008). Thermal effects on the blood respiratory properties of southern bluefin tuna, *Thunnus maccoyii*. *Comp. Biochem. Physiol.* **150A**, 239-246.
Dickson, A. (2010). The carbon dioxide system in seawater: equilibrium chemistry and measurements. In *Guide to Best Practices for Ocean Acidification Research and Data Reporting* (ed. U. Riebesell, V. J. Fabry, L. Hansson and J.-P. Gattuso). Luxembourg: Publications Office of the European Union.
Festa, R. S. and Asakura, T. (1979). Oxygen dissociation curves in children with anemia and malignant disease. *Am. J. Hematol.* **7**, 233-244.
Herbert, N. A., Skov, P. V., Wells, R. M. G. and Steffensen, J. F. (2006). Whole blood-oxygen binding properties of four cold-temperate marine fishes: blood affinity is independent of pH-dependent binding, routine swimming performance, and environmental hypoxia. *Physiol. Biochem. Zool.* **79**, 909-918.
Houlihan, D., Innes, A., Wells, M. and Wells, J. (1982). Oxygen consumption and blood gases of *Octopus vulgaris* in hypoxic conditions. *J. Comp. Physiol. B* **148**, 35-40.
Hüfner, G. (1890). Über das gesetz der dissociation des oxyhaemoglobins und über einige daran sich knüpfende wichtige fragen aus der biologie. *Arch. Anat. Physiol.* **1**, 1-27.
Ikeda, Y., Sugimoto, C., Yonamine, H. and Oshima, Y. (2009). Method of ethanol anaesthesia and individual marking for oval squid (*Sepioteuthis lessoniana* Férussac, 1831 in Lesson 1830-1831). *Aquac. Res.* **41**, 157-160.
Lapennas, G. N. and Lutz, P. L. (1982). Oxygen affinity of sea turtle blood. *Respir. Physiol.* **48**, 59-74.
Lapennas, G. N., Colacino, J. M. and Bonaventura, J. (1981). Thin-layer methods for determination of oxygen binding curves of hemoglobin solutions and blood. In *Methods in Enzymology*, Vol. 76 (ed. E. Chianconi, L. Rossi-Bernardi and E. Antonini), pp. 449-470. London: Academic Press.
Lykkeboe, G. and Johansen, K. (1982). A cephalopod approach to rethinking about the importance of the bohr and haldane effects. *Pac. Sci.* **36**, 305-313.
Mangum, C. P. and Lykkeboe, G. (1979). The influence of inorganic ions and pH on oxygenation properties of the blood in the gastropod mollusc Busycon canaliculatum. *J. Exp. Zool.* **207**, 417-430.
Meir, J. U., Champagne, C. D., Costa, D. P., Williams, C. L. and Ponganis, P. J. (2009). Extreme hypoxemic tolerance and blood oxygen depletion in diving elephant seals. *Am. J. Physiol.* **297**, R927-R939.
Miller, K. I. (1985). Oxygen equilibria of *Octopus dofleini* hemocyanin. *Biochemistry* **24**, 4582-4586.
Morris, S. and Oliver, S. (1999). Respiratory gas transport, haemocyanin function and acid-base balance in *Jasus edwardsii* during emersion and chilling: simulation studies of commercial shipping methods. *Comp. Biochem. Physiol.* **122A**, 309-321.
Morris, S., Taylor, A. C., Bridges, C. R. and Grieshaber, M. K. (1985). Respiratory properties of the haemolymph of the intertidal prawn *Palaemon elegans* (Rathke). *J. Exp. Zool.* **233**, 175-186.
Niesel, W. and Thews, G. (1961). Ein neues verfahren zur schnellen und genauen aufnahme der sauerstoffbindungskurve des blutes und konzentrierter hämoproteidlösungen. *Pflugers Arch.* **273**, 380-395.
Olson, K. N., Hillyer, M. A., Kloss, J. S., Geiselhart, R. J. and Apple, F. S. (2010). Accident or arson: is CO-oximetry reliable for carboxyhemoglobin measurement postmortem? *Clin. Chem.* **56**, 515-519.
Pörtner, H. O. (1990). An analysis of the effects of pH on oxygen binding by squid (*Illex illecebrosus*, *Loligo pealei*) haemocyanin. *J. Exp. Biol.* **150**, 407-424.
PreSens (2004). *Instruction Manual pH-4 mini.* Regensburg, Germany: Precision Sensing GmbH.
PreSens (2012). *Product Sheet for pH Microsensors.* Regensburg, Germany: Precision Sensing GmbH.
R Development Core Team (2013). *R: A Language and Environment for Statistical Computing*. Vienna, Austria: R Foundation for Statistical Computing.
Rasmussen, J. R., Wells, R. M. G., Henty, K., Clark, T. D. and Brittain, T. (2009). Characterization of the hemoglobins of the Australian lungfish *Neoceratodus forsteri* (Krefft). *Comp. Biochem. Physiol.* **152A**, 162-167.
Reeves, R. B. (1980). A rapid micro method for obtaining oxygen equilibrium curves on whole blood. *Respir. Physiol.* **42**, 299-315.
Ritz, C. and Streibig, J. C. (2005). Bioassay analysis using R. *J. Stat. Softw.* **12**, 1-22.
Safavi, A. and Bagheri, M. (2003). Novel optical pH sensor for high and low pH values. *Sens. Actuators B Chem.* **90**, 143-150.
Scott, G. R. (2011). Elevated performance: the unique physiology of birds that fly at high altitudes. *J. Exp. Biol.* **214**, 2455-2462.
Seibel, B., Chausson, F., Lallier, F., Zal, F. and Childress, J. (1999). Vampire blood: respiratory physiology of the vampire squid (Cephalopoda: Vampyromorpha) in relation to the oxygen minimum layer. *Exp. Biol. Online* **4**, 1-10.
Sick, H. and Gersonde, K. (1969). Method for continuous registration of O_2-binding curves of hemoproteins by means of a diffusion chamber. *Anal. Biochem.* **32**, 362-376.
Sick, H. and Gersonde, K. (1972). Theory and application of the diffusion technique for measurement and analysis of O_2-binding properties of very autoxidizable hemoproteins. *Anal. Biochem.* **47**, 46-56.
Truchot, J. P. (1976). Carbon dioxide combining properties of the blood of the shore crab, *Carcinus maenas* (L.): CO_2-dissociation curves and Haldane effect. *J. Comp. Physiol.* **112**, 283-293.
van Holde, K. E., Miller, K. I. and Decker, H. (2001). Hemocyanins and invertebrate evolution. *J. Biol. Chem.* **276**, 15563-15566.
Weber, R. E., Behrens, J. W., Malte, H. and Fago, A. (2008). Thermodynamics of oxygenation-linked proton and lactate binding govern the temperature sensitivity of O2 binding in crustacean (*Carcinus maenas*) hemocyanin. *J. Exp. Biol.* **211**, 1057-1062.
Weber, R. E., Campbell, K. L., Fago, A., Malte, H. and Jensen, F. B. (2010). ATP-induced temperature independence of hemoglobin-O_2 affinity in heterothermic billfish. *J. Exp. Biol.* **213**, 1579-1585.
Wells, M. and Smith, P. (1987). The performance of the octopus circulatory system: a triumph of engineering over design. *Experientia* **43**, 487-499.
Wells, R. M. G. and Weber, R. E. (1989). The measurement of oxygen affinity in blood and haemoglobin solutions. In *Techniques in Comparative Respiratory Physiology: An Experimental Approach* (ed. C. R. Bridges and P. J. Butler), pp. 279-303. Cambridge: Cambridge University Press.
Wirkner, C. S. and Richter, S. (2013). Circulatory system and respiration. *The Natural History of the Crustacea* **1**, 376-412.
Zielinski, S., Sartoris, F. J. and Pörtner, H. O. (2001). Temperature effects on hemocyanin oxygen binding in an antarctic cephalopod. *Biol. Bull.* **200**, 67-76.

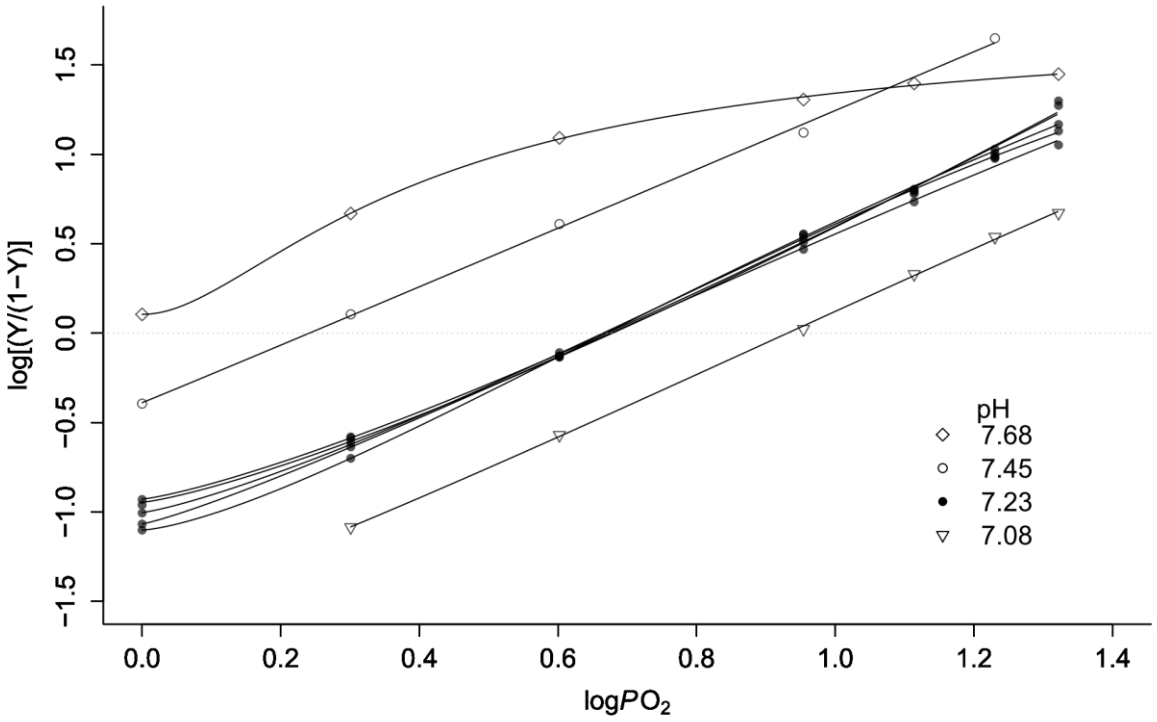

Fig. S1. Hill plot of *Octopus vulgari*s haemolymph measured at 15°C and four different pH. The five replicated measurements at pH 7.23 illustrate low instrumental variability. Lines were fitted using a five parameter logistic model.

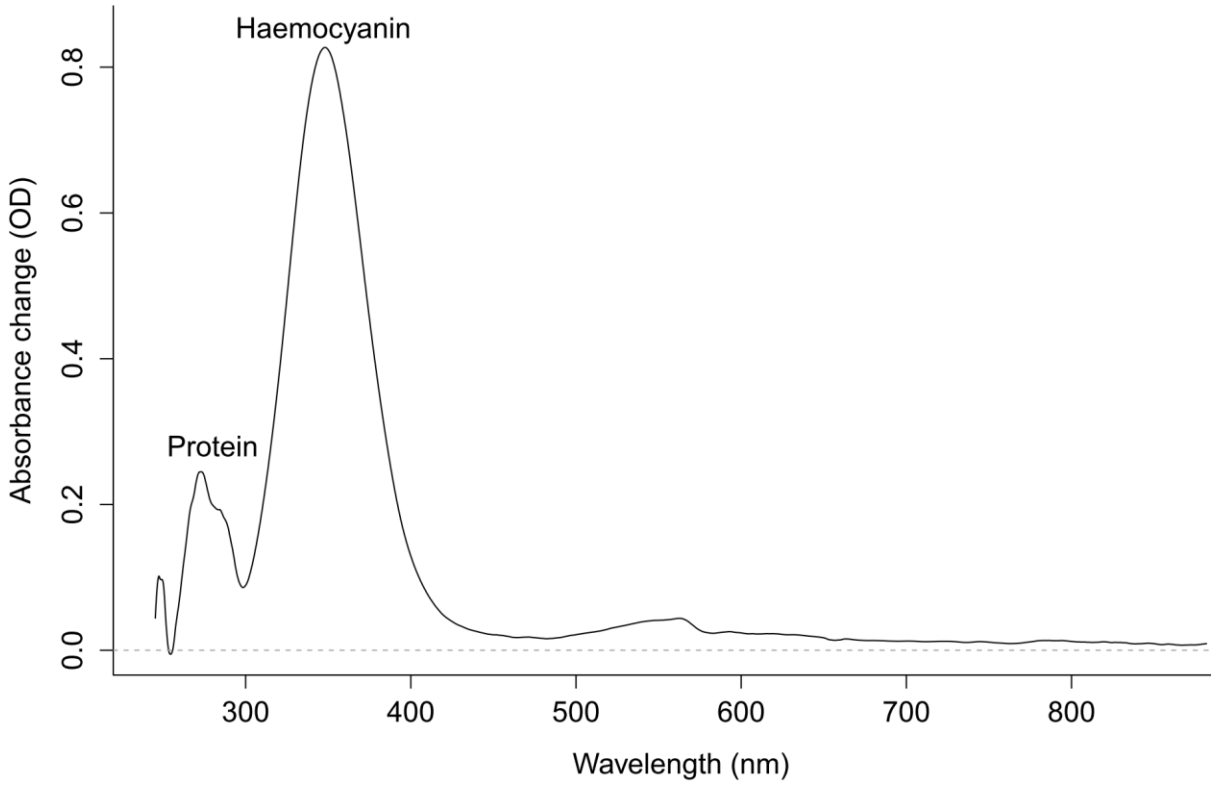

Fig. S2. Subtractive spectrum (absorbance change) of *Octopus vulgaris* haemolymph between the fully deoxygenated (pure nitrogen) and the fully oxygenated state (pure oxygen) determined with 15 µl sample volume at 15°C. Note that pronounced spectral changes not only occur at the haemocyanin peak at 347 nm but also at the protein peak at 280 nm.

Table S1. Currently employed methods to construct oxygen equilibrium curves (OEC).

Method	Characteristics of method	Means to record saturation	Type of temperature control	Range of sample volume	pH determination	PO2 determination	Blood treatment	Time per ODC	Pros	Cons	Example applications
Diffusion chamber	Photospectrometric measurement in chamber equilibrated with gas via diffusion capillaries	Monochromatic / continuous spectrum photospectrometry	Thermostated water bath	3 – 15µl	Measurement with pH capillary electrode (BMS radiometer) in separate sub-sample	Injection of known gas mixture via gas mixing pumps	buffered	10-30 min	Small sample volumes	pH measurements in separate blood sample Low data density	(Weber et al., 1976; Morris et al., 1985; Menze et al., 2005; Harnois et al., 2009; Storz et al., 2009; Campbell et al., 2010)
HEMOX-Analyser	Photospectrometric measurement combined with oxygen sensor	Dual wavelength photospectrometry	Cooling loop connect to thermostated water bath	2 – 50µl	none	Clarke electrode	buffered	30 min	Small samples volumes Very accurate High data density	No pH measurement Recording of only few wavelengths	(Guarnone et al., 1995; Stawski et al., 2006; Biolo et al., 2009; Rasmussen et al., 2009; Cook et al., 2012)
Tonometer	Gas equilibration in glass chamber and external measurement of oxygen tension	Measurement of total O_2 content	Submersion in thermostated water bath	~ 3ml	Measurement of subsample with pH capillary electrode (Radiometer)	Measurement with Clark type electrode	Unbuffered	> 2 hours	Use of native/unbuffered blood	pH measurements in separate blood sample Large sample volumes Low data density	(Pörtner, 1990; Brill et al., 2008)
Thunberg tube / Photometric tonometer	Photospectrometric measurement in cuvette fused with gas equilibrated glass chamber	Monochromatic / continuous spectrum photospectrometry	Immerged into thermostated water bath	~ 3ml	None or in separate blood samples via pH electrodes	Injection of known gas mixture via e.g. gas flow controllers	buffered	> 2 hours	-	No pH measurement or measurement in separate blood sample Large sample volumes Low data density Long equilibration times	(Hill and Wolvekamp, 1936; Olianas et al., 2009; Bonaventura et al., 2010; Seibel, 2012)
Modified cuvette	Photospectrometric measurement in modified cuvette	Continuous spectrum photospectrometry	Temperature controlled cuvette holder	=>400 µl	Simultaneously in same blood sample via immersed micro pH electrode	Injection of known gas mixture via gas mixing pumps	Un-buffered blood	> 4 hours	Direct measurement of pH in same sample Use of native/ unbuffered blood	Large sample volume Long lasting measurements	(Zielinski et al., 2001)
Pwee 50 / HemOscan	Photospectrometric measurement of thin blood films enclosed by Teflon-membranes	Dual wavelength photospectrometry	Temperature controlled chamber (Peltier controller)	1-2µl	Estimated via defined PCO2 and literature or measurement of subsamples with pH capillary electrode (Radiometer)	Injection of known gas mixture via gas mixing pumps or gas flow controller	unbuffered	30-40 min	Small sample volumes	Indirect pH measurement or measurement in separate blood sample Low data density Recording of only few wavelengths	(Clark et al., 2008; Henriksson et al., 2008; Verhille and Farrell, 2012)
CO-Oximeter	Photospectrometric measurement with modified cuvette	3-6 wavelength photospectrometry	none	35-50µl	None or measurement of subsamples with pH capillary electrode (Radiometer)	None / tonometric equilibration with known gas mixtures	unbuffered	20-60 sec per data point	Measures multiple haemoglobin forms	No pH measurement or measurement in separate blood sample Restricted to haemoglobin Low data density	(Jahr et al., 2001)

										Recording of only few wavelengths	
Mixing method	Volumetric mixing of known amounts of fully oxygenated and de-oxygenated blood followed by PO_2 measurement	Setting of O2 saturation by mixing of defined proportions of oxygenated and de-oxygenated blood samples	Immerged into thermostated water bath	Max. 0.8 ml per data point	Measurement with pH capillary electrode (BMS radiometer) or blood gas analyser	Polarographic oxygen electrode via Radiometer (E5046) or Tucker chamber	unbuffered	>50 min per data point	Setting of a desired mixtures allows targeted measurement of e.g. P50 with only a single measurement	Low data density Laborious procedure Time consuming measurement	(Scheid and Meyer, 1978; Meir and Ponganis, 2009; Soegaard et al., 2012)
Tucker chamber	Deoxygenation of blood sample with ferricyanide to release and measure total bound oxygen	Measurement of total bound oxygen	Thermostatically controlled chamber	15-300µl	Measurement with capillary electrode (BMS 2 or PHM 71/73 radiometer)	Polarographic oxygen electrode (Radiometer)	Diluted with saline or unbuffered	>60min	Measurement of total bound oxygen	pH measurements in separate blood sample Low data density	(Tucker, 1967; Herbert et al., 2006; Brill et al., 2008; Petersen and Gamperl, 2011; Leon et al., 2012)

References

Biolo, A., Greferath, R., Siwik, D. A., Qin, F., Valsky, E., Fylaktakidou, K. C., Pothukanuri, S., Duarte, C. D., Schwarz, R. P., Lehn, J.-M. et al. (2009). Enhanced exercise capacity in mice with severe heart failure treated with an allosteric effector of hemoglobin, myo-inositol trispyrophosphate. *Proc. Natl. Acad. Sci. USA* **106**, 1926-1929.

Bonaventura, C., Henkens, R., De Jesus-Bonilla, W., Lopez-Garriga, J., Jia, Y., Alayash, A. I., Siburt, C. J. P. and Crumbliss, A. L. (2010). Extreme differences between hemoglobins I and II of the clam *Lucina pectinalis* in their reactions with nitrite. *BBA-Proteins Proteom.* **1804**, 1988-1995.

Brill, R., Bushnell, P., Schroff, S., Seifert, R. and Galvin, M. (2008). Effects of anaerobic exercise accompanying catch-and-release fishing on blood-oxygen affinity of the sandbar shark (*Carcharhinus plumbeus*, Nardo). *J. Exp. Mar. Biol. Ecol.* **354**, 132-143.

Campbell, K. L., Roberts, J. E., Watson, L. N., Stetefeld, J., Sloan, A. M., Signore, A. V., Howatt, J. W., Tame, J. R., Rohland, N., Shen, T. J. et al. (2010). Substitutions in woolly mammoth hemoglobin confer biochemical properties adaptive for cold tolerance. *Nat. Genet.* **42**, 536-540.

Clark, T. D., Seymour, R. S., Wells, R. M. G. and Frappell, P. B. (2008). Thermal effects on the blood respiratory properties of southern bluefin tuna, *Thunnus maccoyii*. *Comp. Biochem. Physiol. Part A Mol. Integr. Physiol.* **150**, 239-246.

Cook, D. G., Iftikar, F. I., Baker, D. W., Hickey, A. J. R. and Herbert, N. A. (2012). Low O2 acclimation shifts the hypoxia avoidance behaviour of snapper (*Pagrus auratus*) with only subtle changes in aerobic and anaerobic function. *J. Exp. Biol.*

Guarnone, R., Centenara, E. and Barosi, G. (1995). Performance characteristics of Hemox-Analyzer for assessment of the hemoglobin dissociation curve. *Haematologica* **80**, 426-430.

Harnois, T., Rousselot, M., Rogniaux, H. and Zal, F. (2009). High-level production of recombinant *Arenicola marina* globin chains in *Escherichia coli*: A new generation of blood substitute. *Artif. Cells Blood Substit. Biotechnol.* **37**, 106-116.

Henriksson, P., Mandic, M. and Richards, J. G. (2008). The osmorespiratory compromise in sculpins: impaired gas exchange is associated with freshwater tolerance. *Physiol. Biochem. Zool.* **81**, 310-319.

Herbert, Neill A., Skov, Peter V., Wells, Rufus M. G. and Steffensen, John F. (2006). Whole blood–oxygen binding properties of four cold-temperate marine fishes: Blood affinity is independent of pH-dependent binding, routine swimming performance, and environmental hypoxia. *Physiol. Biochem. Zool.* **79**, 909-918.

Hill, R. and Wolvekamp, H. P. (1936). The oxygen dissociation curve of haemoglobin in dilute solution. *Proc. R. Soc. Lond. B Biol. Sci.* **120**, 484-495.

Jahr, J. S., Driessen, B., Lurie, F., Tang, Z., Louie, R. F. and Kost, G. (2001). Oxygen saturation measurements in canine blood containing hemoglobin glutamer-200 (bovine): In vitro validation of the NOVA CO-Oximeter. *Vet. Clin. Pathol.* **30**, 39-45.

Leon, K., Pichavant-Rafini, K., Quemener, E., Sebert, P., Egreteau, P. Y., Ollivier, H., Carre, J. L. and L'Her, E. (2012). Oxygen blood transport during experimental sepsis: effect of hypothermia*. *Crit Care Med* **40**, 912-918.

Meir, J. U. and Ponganis, P. J. (2009). High-affinity hemoglobin and blood oxygen saturation in diving emperor penguins. *J. Exp. Biol.* **212**, 3330-3338.

Menze, M. A., Hellmann, N., Decker, H. and Grieshaber, M. K. (2005). Allosteric models for multimeric proteins: Oxygen-linked effector binding in hemocyanin†. *Biochemistry* **44**, 10328-10338.

Morris, S., Taylor, A. C., Bridges, C. R. and Grieshaber, M. K. (1985). Respiratory properties of the haemolymph of the intertidal prawn *Palaemon elegans* (Rathke). *J. Exp. Zool.* **233**, 175-186.

Olianas, A., Manconi, B., Masia, D., Sanna, M. T., Castagnola, M., Salvadori, S., Messana, I., Giardina, B. and Pellegrini, M. (2009). The oxygen-binding modulation of hemocyanin from the Southern spiny lobster *Palinurus gilchristi*. *J. Comp. Physiol. B* **179**, 193-203.

Petersen, L. H. and Gamperl, A. K. (2011). Cod (*Gadus morhua*) cardiorespiratory physiology and hypoxia tolerance following acclimation to low-oxygen conditions. *Physiol. Biochem. Zool.* **84**, 18-31.

Pörtner, H. O. (1990). An analysis of the effects of pH on oxygen binding by squid (Illex illecebrosus, *Loligo pealei*) haemocyanin. *J. Exp. Biol.* **150**, 407.
Rasmussen, J. R., Wells, R. M. G., Henty, K., Clark, T. D. and Brittain, T. (2009). Characterization of the hemoglobins of the Australian lungfish *Neoceratodus forsteri* (Krefft). *Comp. Biochem. Physiol., A: Comp. Physiol.* **152**, 162-167.
Scheid, P. and Meyer, M. (1978). Mixing technique for study of oxygen-hemoglobin equilibrium: a critical evaluation. *J. Appl. Physiol.* **45**, 818-822.
Seibel, B. A. (2012). The jumbo squid, *Dosidicus gigas* (Ommastrephidae), living in oxygen minimum zones II: Blood-oxygen binding. *Deep-Sea Res. Pt. II*.
Soegaard, L. B., Hansen, M. N., van Elk, C., Brahm, J. and Jensen, F. B. (2012). Respiratory properties of blood in the harbor porpoise, *Phocoena phocoena*. *J. Exp. Biol.* **215**, 1938-1943.
Stawski, C. Y., Grigg, G. C., Booth, D. T. and Beard, L. A. (2006). Temperature and the respiratory properties of whole blood in two reptiles, *Pogona barbata* and *Emydura signata*. *Comp. Biochem. Physiol. Part A Mol. Integr. Physiol.* **143**, 173-183.
Storz, J. F., Runck, A. M., Sabatino, S. J., Kelly, J. K., Ferrand, N., Moriyama, H., Weber, R. E. and Fago, A. (2009). Evolutionary and functional insights into the mechanism underlying high-altitude adaptation of deer mouse hemoglobin. *Proc. Natl. Acad. Sci. USA* **106**, 14450-14455.
Tucker, V. A. (1967). Method for oxygen content and dissociation curves on microliter blood samples. *J. Appl. Physiol.* **23**, 410-414.
Verhille, C. and Farrell, A. P. (2012). The in vitro blood-O2 affinity of triploid rainbow trout *Oncorhynchus mykiss* at different temperatures and CO2 tensions. *J. Fish Biol.* **81**, 1124-1132.
Weber, R. E., Lykkeboe, G. and Johansen, K. (1976). Physiological properties of eel haemoglobin: hypoxic acclimation, phosphate effects and multiplicity. *J. Exp. Biol.* **64**, 75-88.
Zielinski, S., Sartoris, F. J. and Pörtner, H. O. (2001). Temperature effects on hemocyanin oxygen binding in an Antarctic cephalopod. *Biol. Bull. (Woods Hole)* **200**, 67-76.

Table S2. Detailed description of diffusion chamber components

#	Component	Description
1	Collimating lenses	The collimating lenses form a straight light beam penetrating the sample droplet.
2	Control panel for gas inflow	The control panel contains multiple gas inlets to connect up to six types of gases (e.g. N_2, O_2, CO_2). In this study only one inlet was used and connected to a Wösthoff gas mixing pump, which supplied the desired gas mixture. Each inlet has one adjustable valve to regulate the incoming gas pressure.
3	Control wheel for gas distribution	Control wheel that directs the gas flow via a copper tube from a particular gas washing flask/gas (19) inlet to the sample chamber
4	Upper lens holder	The custom made upper plastic lens holder positions a collimating lens (1) connected to a fiber optic cable on top of the sample droplet.
5	Central metal block	The metal block contains the sample chamber and holds the sample holder (16) with the sample droplet and the pH optode (9). The metal block is ventrally penetrated by the central cylinder (14) to allow the passage of light through the sample. The metal itself allows fast temperature equilibration between the samples chamber and the surrounding medium.
6	Pressure balance tube	Tube that releases excess gas supplied by gas mixing pumps to avoid overpressure in the sample chamber.
7	Water disperser	The water disperser is connected to an external thermostatted water bath and assures rigorous mixing of water.
8	Gas dispersing membrane	Sponge-type membrane that disperses inflowing dry gas into temperature equilibrated water on top of the membrane.
9	pH optode	Micro pH optode that fitted onto the sample holder (16) to measure pH of the sample droplet
10	Lens spacer	The lens spacer is screwed on top of the lower lens holder (11) to assure a minimum distance of 10mm to the sample glass plate. The spacer also presses against the sample slide if the lower lens holder (11) is moved upwards, which seals the sample chamber from the surrounding gas atmosphere.
11	Lower lens holder	The custom made lower plastic lens holder positions a collimating lens (1) connected to a fiber optic cable below the sample droplet.
12	Locking bushing	Ring that moves the lower lens holder (11) upwards upon turning to fix the sample holder (16).
13	Sealing rings	The rubber sealing rings prevent gas leakage from the surrounding atmosphere into the sample chamber.
14	Central cylinder	The central hollow metal cylinder forms the light channel for the absorbance measurement and houses the upper (4) and lower (11) lens holders.
15	Water reservoir	Can be connected to a thermostatted water bath via insolated hoses, which circulates water or water mixed with anti-freeze agent to equilibrate all diffusion chamber components to the experimental temperature.
16	Sample holder	Plastic samples holder that carries the sample glass plate with the sample droplet at its end as well as the pH optode (9). The sample holder is moved into the central metal block (5) to position the sample droplet into the light beam in the center of the diffusion chamber.
17	Tygon® tubings	Gas tight tubings (CM Scientific Ltd., Silsden, U.K.) that connect the gas inlets with the gas-washing flasks (19) and the gas distributor (3).
18	Diffusion chamber housing	The housing of the diffusion chamber is made of acrylic glass and fixed with regular spaced metal screws. The inner sides are sealed with aquarium

		sealing.
19	Gas-washing flask	The gas-washing flasks are composed of glass humidify the incoming gas to prevent drying and temperature changes of the sample droplet.
20	Thermostat connectors	To connect the water bath to an external circulating thermostatted water bath.
21	Temperature sensor	External temperature sensor connected to the pH recorder to monitor the temperature of the diffusion chamber during measurements.
22	Fiber optic cable	Fiber optic cable from the UV-VIS light source fixed to the collimating lens (1) and housed in the upper lens holder (4).

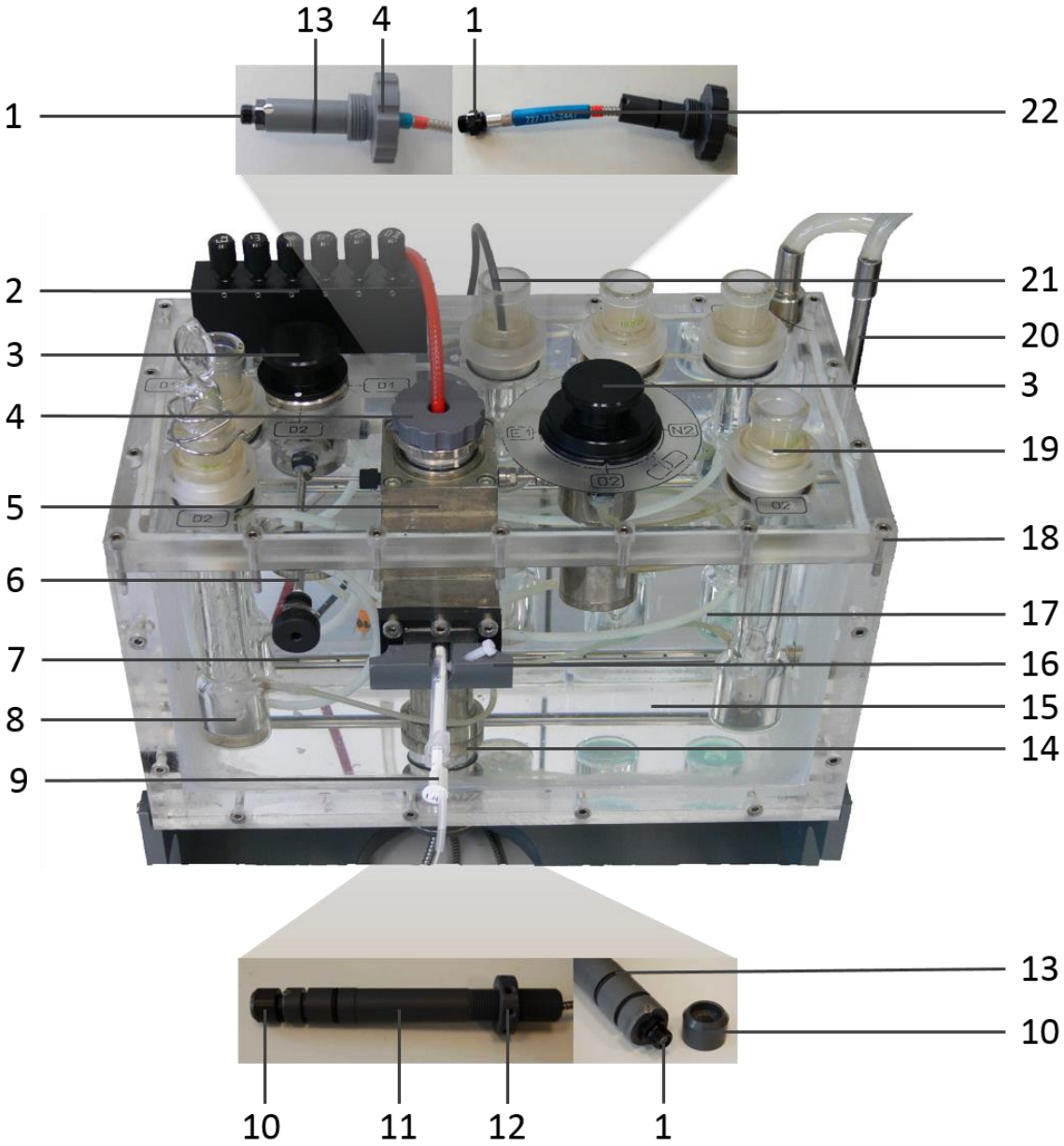

Table S3. References used to analyse data density of oxygen dissociation curves from various methods

Method	**References**
Modified diffusion chamber	This study
HEMOX-analyser	(Stawski et al., 2006; Cabrales et al., 2008; Biolo et al., 2009; Liu et al., 2009; Liu et al., 2010)
Modified cuvette	(Zielinski et al., 2001)
Pwee 50 / HemOscan	(Clark et al., 2008; Bianchini, 2012; Verhille and Farrell, 2012)
Thunberg tube / Spectrophotometric tonometer	(Hill and Wolvekamp, 1936; Nakagawa et al., 2005; Olianas et al., 2009; Bonaventura et al., 2010; Seibel, 2012)
Mixing method	(Scheid and Meyer, 1978; Boutilier et al., 2000; Soncini and Glass, 2000; de Salvo Souza et al., 2001; Meir and Ponganis, 2009)
CO-Oximeter	(Bunn et al., 1972; Lokich et al., 1973; Elbaum et al., 1974; Harms et al., 1998; Jahr et al., 2001)
Diffusion chamber	(Morris et al., 1985; Menze et al., 2005; Broekman et al., 2006; Rutjes et al., 2007; Sugumar and Munuswamy, 2007; Storz et al., 2009)
Tucker chamber	(Bridges et al., 1979; Airaksinen and Nikinmaa, 1995; Gollock et al., 2006; Brill et al., 2008; Petersen and Gamperl, 2011; Leon et al., 2012)

References

Airaksinen, S. and Nikinmaa, M. (1995). Effect of haemoglobin concentration on the oxygen affinity of intact lamprey erythrocytes. *J. Exp. Biol.* **198**, 2393-2396.

Bianchini, K. (2012). The ontogeny of blood oxygen transport and the hypoxia response in early life stages of the rainbow trout, *Oncorhynchus mykiss*. In *Department of Integrative Biology*, vol. Master of Science, pp. 103. Guelph, Ontario, Canada: University of Guelph.

Biolo, A., Greferath, R., Siwik, D. A., Qin, F., Valsky, E., Fylaktakidou, K. C., Pothukanuri, S., Duarte, C. D., Schwarz, R. P., Lehn, J.-M. et al. (2009). Enhanced exercise capacity in mice with severe heart failure treated with an allosteric effector of hemoglobin, myo-inositol trispyrophosphate. *Proc. Natl. Acad. Sci. USA* **106**, 1926-1929.

Bonaventura, C., Henkens, R., De Jesus-Bonilla, W., Lopez-Garriga, J., Jia, Y., Alayash, A. I., Siburt, C. J. P. and Crumbliss, A. L. (2010). Extreme differences between hemoglobins I and II of the clam *Lucina pectinalis* in their reactions with nitrite. *BBA-Proteins Proteom.* **1804**, 1988-1995.

Boutilier, R. G., West, T. G., Webber, D. M., Pogson, G. H., Mesa, K. A., Wells, J. and Wells, M. J. (2000). The protective effects of hypoxia-induced hypometabolism in the Nautilus. *J. Comp. Physiol. B* **170**, 261-268.

Bridges, C., Bicudo, J. and Lykkeboe, G. (1979). Oxygen content measurement in blood containing haemocyanin. *Comp. Biochem. Physiol. A Physiol.* **62**, 457-461.

Brill, R., Bushnell, P., Schroff, S., Seifert, R. and Galvin, M. (2008). Effects of anaerobic exercise accompanying catch-and-release fishing on blood-oxygen affinity of the sandbar shark (*Carcharhinus plumbeus*, Nardo). *J. Exp. Mar. Biol. Ecol.* **354**, 132-143.

Broekman, M. S., Bennett, N. C., Jackson, C. R. and Weber, R. E. (2006). Does altitudinal difference modulate the respiratory properties in subterranean rodents' (*Cryptomys hottentotus mahali*) blood? *Physiol. Behav.* **88**, 77-81.

Bunn, H. F., Meriwether, W. D., Balcerzak, S. P. and Rucknagel, D. L. (1972). Oxygen equilibrium of hemoglobin E. *J. Clin. Investig.* **51**, 2984.

Cabrales, P., Tsai, A. G. and Intaglietta, M. (2008). Modulation of perfusion and oxygenation by red blood cell oxygen affinity during acute anemia. *Am. J. Respir. Cell Mol. Biol.* **38**, 354.

Clark, T. D., Seymour, R. S., Wells, R. M. G. and Frappell, P. B. (2008). Thermal effects on the blood respiratory properties of southern bluefin tuna, *Thunnus maccoyii*. *Comp. Biochem. Physiol. Part A Mol. Integr. Physiol.* **150**, 239-246.

de Salvo Souza, R., Soncini, R., Glass, M., Sanches, J. and Rantin, F. (2001). Ventilation, gill perfusion and blood gases in dourado, *Salminus maxillosus* Valenciennes (Teleostei, Characidae), exposed to graded hypoxia. *J. Comp. Physiol. B* **171**, 483-489.

Elbaum, D., Nagel, R. L., Bookchin, R. M. and Herskovits, T. T. (1974). Effect of alkylureas on the polymerization of hemoglobins. *Proc. Natl. Acad. Sci. USA* **71**, 4718-4722.

Gollock, M. J., Currie, S., Petersen, L. H. and Gamperl, A. K. (2006). Cardiovascular and haematological responses of Atlantic cod (*Gadus morhua*) to acute temperature increase. *J. Exp. Biol.* **209**, 2961-2970.

Harms, C. A., McClaran, S. R., Nickele, G. A., Pegelow, D. F., Nelson, W. B. and Dempsey, J. A. (1998). Exercise-induced arterial hypoxaemia in healthy young women. *J. Physiol.* **507**, 619-628.

Hill, R. and Wolvekamp, H. P. (1936). The oxygen dissociation curve of haemoglobin in dilute solution. *Proc. R. Soc. Lond. B Biol. Sci.* **120**, 484-495.

Jahr, J. S., Driessen, B., Lurie, F., Tang, Z., Louie, R. F. and Kost, G. (2001). Oxygen saturation measurements in canine blood containing hemoglobin glutamer-200 (bovine): In vitro validation of the NOVA CO-Oximeter. *Vet. Clin. Pathol.* **30**, 39-45.

Leon, K., Pichavant-Rafini, K., Quemener, E., Sebert, P., Egreteau, P. Y., Ollivier, H., Carre, J. L. and L'Her, E. (2012). Oxygen blood transport during experimental sepsis: effect of hypothermia*. *Crit Care Med* **40**, 912-918.

Liu, C., Zhang, L. F., Song, M. L., Bao, H. G., Zhao, C. J. and Li, N. (2009). Highly efficient dissociation of oxygen from hemoglobin in Tibetan chicken embryos compared with lowland chicken embryos incubated in hypoxia. *Poult. Sci.* **88**, 2689-2694.

Liu, Y.-x., Yue, W., Ji, L., Nan, X. and Pei, X.-t. (2010). Production of erythriod cells from human embryonic stem cells by fetal liver cell extract treatment. *BMC Dev. Biol.* **10**, 85.

Lokich, J. J., Moloney, W. C., Bunn, H. F., Bruckheimer, S. M. and Ranney, H. M. (1973). Hemoglobin brigham (alpha2Abeta2100 Pro-->Leu). Hemoglobin variant associated with familial erythrocytosis. *J. Clin. Invest.* **52**, 2060-2067.

Meir, J. U. and Ponganis, P. J. (2009). High-affinity hemoglobin and blood oxygen saturation in diving emperor penguins. *J. Exp. Biol.* **212**, 3330-3338.

Menze, M. A., Hellmann, N., Decker, H. and Grieshaber, M. K. (2005). Allosteric models for multimeric proteins: Oxygen-linked effector binding in hemocyanin†. *Biochemistry* **44**, 10328-10338.

Morris, S., Taylor, A. C., Bridges, C. R. and Grieshaber, M. K. (1985). Respiratory properties of the haemolymph of the intertidal prawn *Palaemon elegans* (Rathke). *J. Exp. Zool.* **233**, 175-186.

Nakagawa, T., Onoda, S., Kanemori, M., Sasayama, Y. and Fukumori, Y. (2005). Purification, characterization and sequence analyses of the extracellular giant hemoglobin from *Oligobrachia mashikoi*. *Zool Sci* **22**, 283-291.

Olianas, A., Manconi, B., Masia, D., Sanna, M. T., Castagnola, M., Salvadori, S., Messana, I., Giardina, B. and Pellegrini, M. (2009). The oxygen-binding modulation of hemocyanin from the Southern spiny lobster *Palinurus gilchristi*. *J. Comp. Physiol. B* **179**, 193-203.

Petersen, L. H. and Gamperl, A. K. (2011). Cod (*Gadus morhua*) cardiorespiratory physiology and hypoxia tolerance following acclimation to low-oxygen conditions. *Physiol. Biochem. Zool.* **84**, 18-31.

Rutjes, H. A., Nieveen, M. C., Weber, R. E., Witte, F. and Van den Thillart, G. E. E. J. M. (2007). Multiple strategies of Lake Victoria cichlids to cope with lifelong hypoxia include hemoglobin switching. *Am. J. Physiol. Regul. Integr. Comp. Physiol.* **293**, R1376-R1383.

Scheid, P. and Meyer, M. (1978). Mixing technique for study of oxygen-hemoglobin equilibrium: a critical evaluation. *J. Appl. Physiol.* **45**, 818-822.

Seibel, B. A. (2012). The jumbo squid, *Dosidicus gigas* (Ommastrephidae), living in oxygen minimum zones II: Blood-oxygen binding. *Deep-Sea Res. Pt. II*.

Soncini, R. and Glass, M. L. (2000). Oxygen and acid-base status related drives to gill ventilation in carp. *J. Fish Biol.* **56**, 528-541.

Stawski, C. Y., Grigg, G. C., Booth, D. T. and Beard, L. A. (2006). Temperature and the respiratory properties of whole blood in two reptiles, *Pogona barbata* and *Emydura signata*. *Comp. Biochem. Physiol. Part A Mol. Integr. Physiol.* **143**, 173-183.

Storz, J. F., Runck, A. M., Sabatino, S. J., Kelly, J. K., Ferrand, N., Moriyama, H., Weber, R. E. and Fago, A. (2009). Evolutionary and functional insights into the mechanism underlying high-altitude adaptation of deer mouse hemoglobin. *Proc. Natl. Acad. Sci. USA* **106**, 14450-14455.

Sugumar, V. and Munuswamy, N. (2007). Physical, biochemical and functional characterization of haemoglobin from three strains of Artemia. *Comp. Biochem. Physiol. Part A Mol. Integr. Physiol.* **146**, 291-298.

Verhille, C. and Farrell, A. P. (2012). The in vitro blood-O2 affinity of triploid rainbow trout *Oncorhynchus mykiss* at different temperatures and CO2 tensions. *J. Fish Biol.* **81**, 1124-1132.

Zielinski, S., Sartoris, F. J. and Pörtner, H. O. (2001). Temperature effects on hemocyanin oxygen binding in an Antarctic cephalopod. *Biol. Bull. (Woods Hole)* **200**, 67-76.